Deconvolution with Correct Sampling

P. MAGAIN[1,], F. COURBIN[1,2], S. SOHY[1]*

[1]Institut d'Astrophysique, Université de Liège, Belgium
[2]URA 173 CNRS-DAEC, Observatoire de Paris-Meudon, France
**Also Maître de Recherches au Fonds National de la Recherche Scientifique (Belgium)*

1. Deconvolution

Much effort is presently devoted to the improvement of the spatial resolution of astronomical images, either via the introduction of new observing techniques (as interferometry or adaptive optics) or via a subsequent numerical processing of the image (deconvolution).

In the following, we briefly describe the basic ideas behind a new deconvolution technique which overcomes some of the drawbacks of the traditional methods and which gives results of high photometric and astrometric accuracy. We also show how it can be combined with other techniques (e.g. adaptive optics) to give even better results.

An observed image may usually be mathematically expressed as a convolution of the original light distribution with the "total instrumental profile" – the latter being the image of a point source obtained with the instrument considered, including the atmospheric seeing if the telescope is ground-based. The total blurring function is called the *Point Spread Function* (PSF) of the image.

Thus, the imaging equation may be written:

$$d(\vec{x}) = t(\vec{x}) * f(\vec{x}) + n(\vec{x}) \qquad (1)$$

where $f(\vec{x})$ and $d(\vec{x})$ are the original and observed light distributions, $t(\vec{x})$ is the total PSF and $n(\vec{x})$ the measurement errors *(noise)* affecting the data.

The aim of deconvolution may be stated in the following way: given the observed image $d(\vec{x})$ and the PSF $t(\vec{x})$, recover the original light distribution $f(\vec{x})$. Being an inverse problem, deconvolution is also an ill-posed problem, and no unique solution can be found, especially in the presence of noise. This is due to the fact that many light distributions are, after convolution with the PSF, compatible within the error bars with the observed image. Therefore, regularisation techniques have to be used in order to select a plausible solution amongst the family of possible ones and a large variety of deconvolution methods have been proposed, depending on the way this particular solution is chosen (in

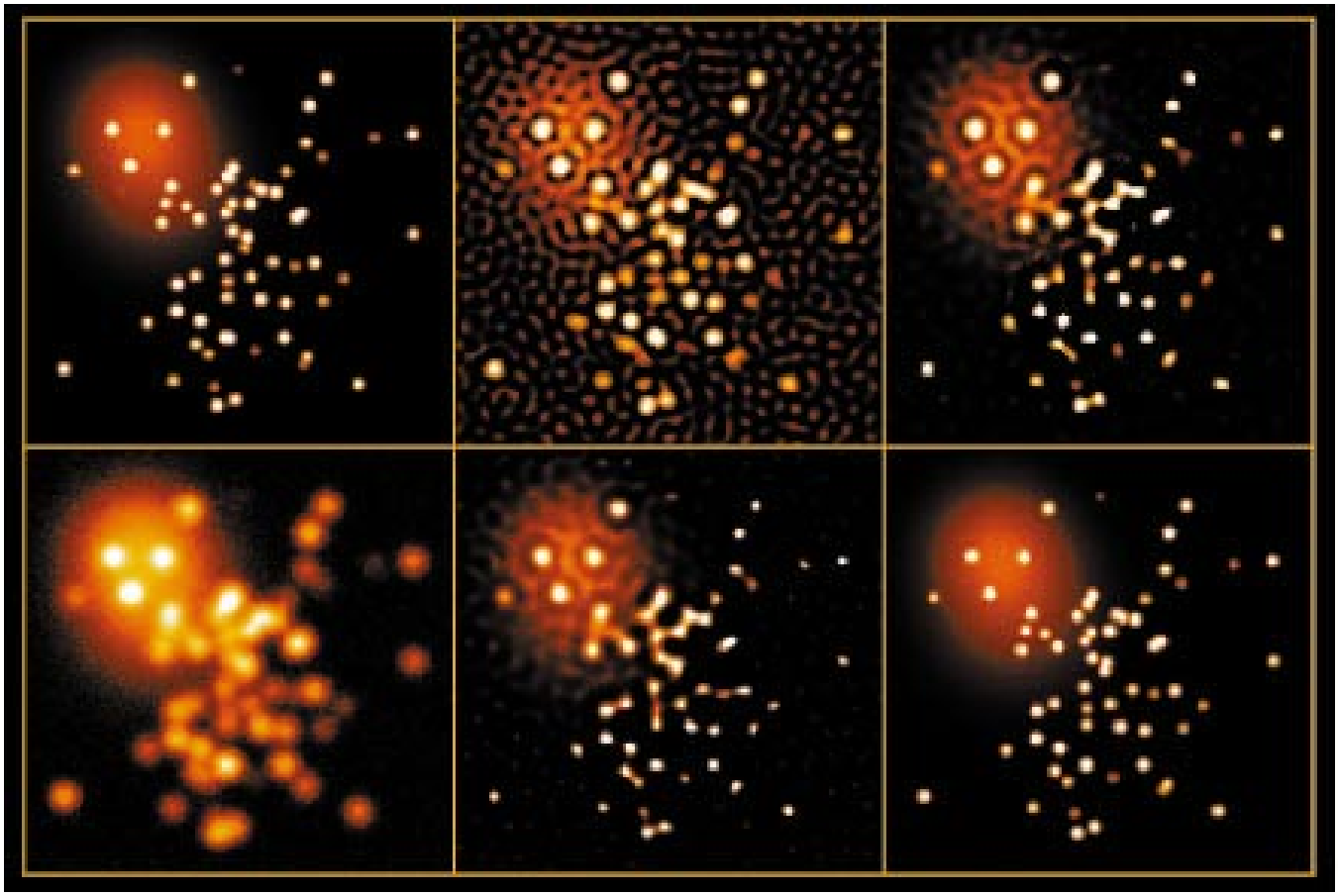

Figure 1: Deconvolution of a simulated image of a star cluster partly superimposed on a background galaxy. Top left: true light distribution with 2 pixels FWHM resolution; bottom left: observed image with 6 pixels FWHM and noise; top middle: Wiener filter deconvolution of the observed image; bottom middle: 50 iterations of the accelerated Richardson-Lucy algorithm; top right: maximum entropy deconvolution; bottom right: deconvolution with our new algorithm.

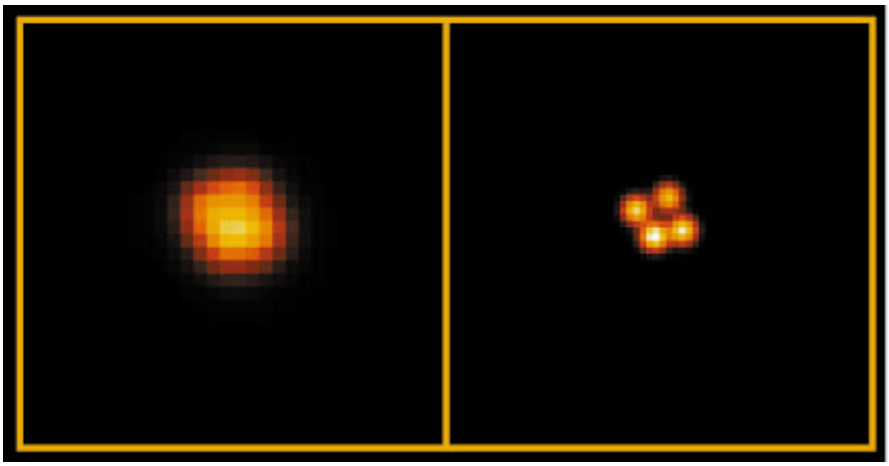

Figure 2: Deconvolution of a pre-discovery image of the Cloverleaf gravitational mirage obtained with the ESO/MPI 2.2-m telescope at La Silla (Chile). Left: observed image with a FWHM resolution of 1.3 arcsec; right: our deconvolution with improved sampling and a FWHM resolution of 0.5 arcsec.

general, the selected solution is the smoothest according to some pre-defined criterion, e.g., the image with the largest entropy).

In order to choose the correct answer in the family of possible solutions to this inverse problem, it is also very useful to consider any available *prior knowledge.* One such prior knowledge is the *positivity* of the light distribution: no negative light flux can be recorded, so that all solutions with negative values may be rejected. The maximum entropy method automatically ensures positivity of the solution. This is also the case, under certain conditions, for other popular methods, such as the Richardson-Lucy iterative algorithm (Richardson, 1972; Lucy, 1974).

However, most of the known deconvolution algorithms suffer from a number of weak points which strongly limit their usefulness. The two most important problems in this respect are the following: (1) traditional deconvolution methods tend to produce artefacts in some instances (e.g. oscillations in the vicinity of image discontinuities, or around point sources superimposed on a smooth background); (2) the relative intensities of different parts of the image (e.g. different stars) are not conserved, thus precluding any photometric measurements. In the following, we identify the main cause of these problems and show how to circumvent it.

2. Sampling

The sampling theorem (Shannon, 1949, Press et al., 1989) determines the maximal sampling interval allowed so that an entire function can be reconstructed from sampled data.

The imaging instruments are generally designed so that the sampling theorem is approximately fulfilled in average observing conditions. A typical sampling encountered is ~ 2 sampling intervals per FWHM of the PSF (this does not ensure good sampling for high S/N images, but is roughly sufficient at low S/N).

The main problem with classical deconvolution algorithms is the following: *if the observed data are sampled so that they just obey the sampling theorem, the deconvolved data will generally violate that same theorem.* Indeed, increasing the resolution means recovering highest Fourier frequencies, so that the correct sampling would become denser.

This is particularly true if the image contains point sources, which is generally the case for astronomical images. Indeed, the angular diameters of most stars ($\ll 0.001$ arcsec) are so small compared to the sampling interval (~ 0.1 arcsec) that they may be considered as point sources ("δ-functions"). In such an instance, it would be hopeless to reduce the sampling interval in an attempt to obtain a good sampling of such "δ-functions".

This is the source of some of the artefacts present in the deconvolved images and, in particular, of the "ringing" around point sources superimposed on a diffuse background. The origin of this "ringing" may be intuitively understood in the following way.

If a point source is located between two sampling points (as will generally be the case), in order to correctly reproduce its position, the deconvolution algorithm will have to distribute its intensity over several sampling points. But, then, the width of the source will be too large and ringing will appear as the algorithm attempts to decrease the intensity on the edges of the reconstructed source, in order to keep the re-convolved model as close as possible to the observed data.

In fact, it is not possible to correctly reproduce both the position and the width of a sampled point source. To reproduce the zero width, the full signal must be concentrated on a single sampling point. On the other hand, to reproduce the position with a precision which is better than the sampling interval, the signal has to be distributed over several points.

3. Solution

The correct approach to this sampling problem is thus *not* to deconvolve with the total PSF $t(\vec{x})$, but rather with a narrower function $s(\vec{x})$ chosen so that the deconvolved image has its own PSF $r(\vec{x})$ compatible with the adopted sampling. These three functions are simply related by:

$$t(\vec{x}) = r(\vec{x}) * s(\vec{x}) \qquad (2)$$

The shape and width of $r(\vec{x})$ can be chosen by the user. The only constraint is that Eq. (2) admits a solution $s(\vec{x})$. The function $s(\vec{x})$ by which the observed image has to be deconvolved is thus obtained as the deconvolution of the total PSF $t(\vec{x})$ by the final PSF $r(\vec{x})$. Of course, the sampling interval of the deconvolved image does not need to be equal to the sampling interval of the

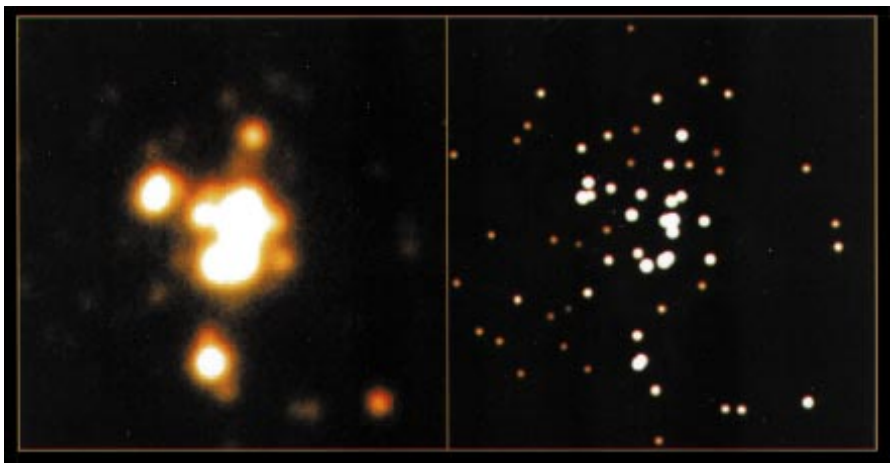

Figure 3: Deconvolution of an image of the compact star cluster Sk 157 in the Small Magellanic Cloud. Left: image obtained with the ESO/MPI 2.2-m telescope at La Silla (1.1 arcsec FWHM); right: deconvolution with our algorithm (0.26 arcsec FWHM).

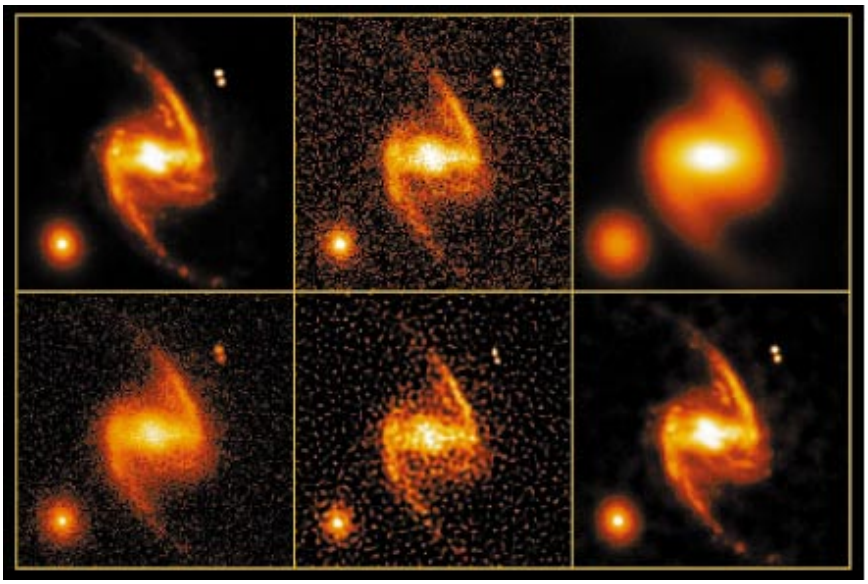

Figure 4: Simultaneous deconvolution of simulated images. Top left: true light distribution with 2 pixels FWHM resolution; top middle: image obtained with a space telescope; top right: image obtained with a large ground-based telescope; bottom left: sum of the two images; bottom middle: simultaneous deconvolution with Lucy's algorithm; bottom right: simultaneous deconvolution with our new algorithm.

original image, so that $r(\vec{x})$ may be much narrower than $t(\vec{x})$, even if the original sampling would not allow it.

Thus, the deconvolution algorithm should not attempt to determine the light distribution as if it were obtained with an *ideal* instrument (e.g. a space telescope with a primary mirror of infinite size). This is forbidden as long as the data are sampled. Rather, the aim of deconvolution should be to determine the light distribution as if it were observed with a *better* instrument (e.g. a 10-m space telescope).

Deconvolution by $s(\vec{x})$ ensures that the solution will not violate the sampling theorem. It also has a very important additional advantage: if the image contains point sources, their shape in the deconvolved image is now precisely known: it is simply $r(\vec{x})$. This is a very strong *prior knowledge,* and it may be used to constrain the solution $f(\vec{x})$, which can be written as the sum of smooth background plus a number of point sources, whose intensities and positions are unknown.

Another prior knowledge can be used to constrain the solution: indeed, the background itself should not contain any Fourier component with frequency higher than allowed by the final deconvolved PSF $r(\vec{x})$, and this knowledge can be used to force smoothness on the scale length of $r(\vec{x})$.

4. Examples

Figure 1 compares the results of our new deconvolution algorithm to those of three classical methods in the case of a simulated star cluster partly superimposed on a smooth background (e.g. a

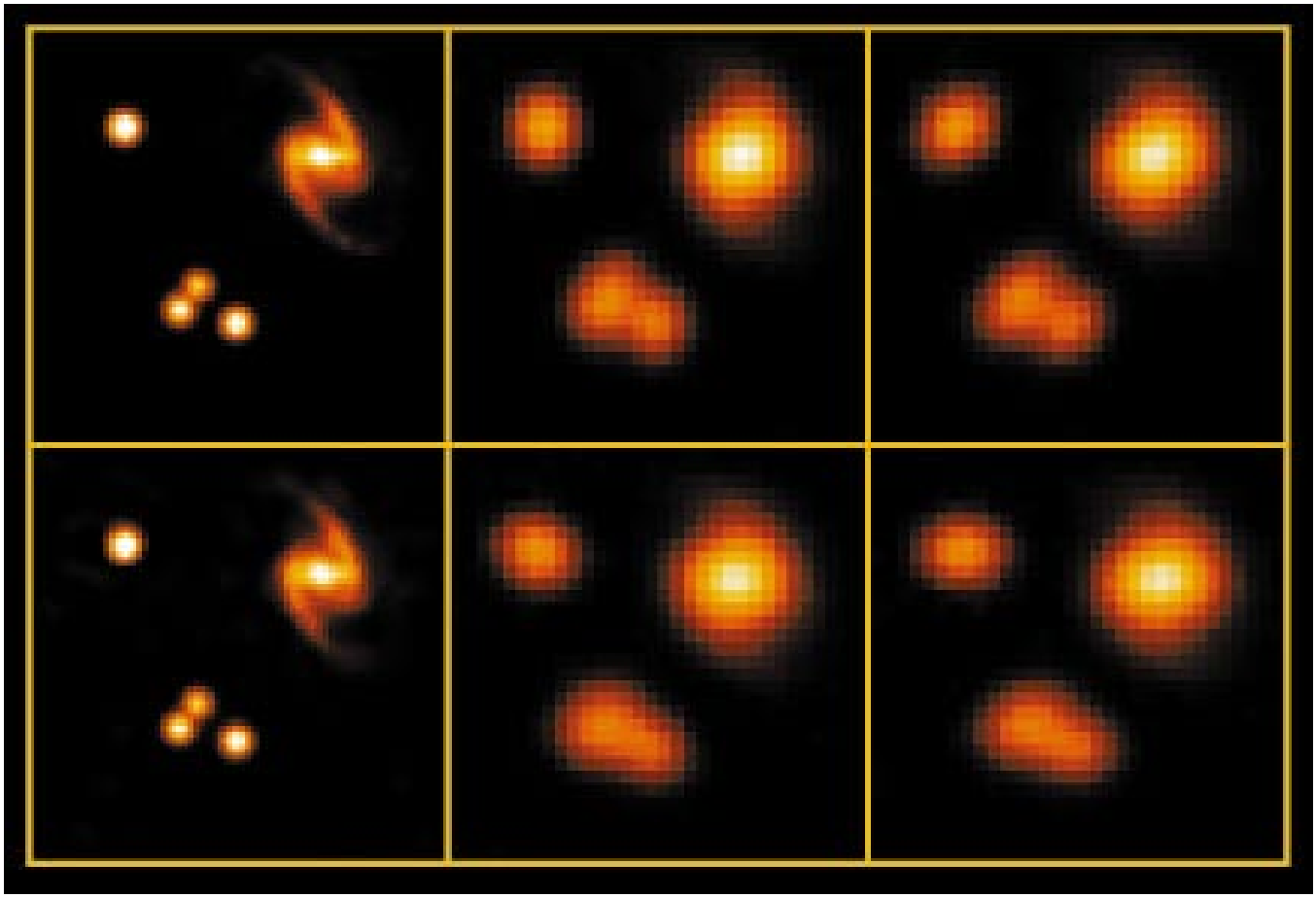

Figure 5: Simultaneous deconvolution of 4 simulated adaptive-optics-like images. Top left: true light distribution with 2 pixels FWHM resolution; middle and right: 4 images obtained with the same instrument but in varying atmospheric conditions; bottom left: simultaneous deconvolution with our new algorithm.

distant elliptical galaxy). It is clear that our result is free from the artefacts present in the other methods and that it allows an accurate reconstruction of the original light distribution.

An application to real astronomical data is shown on Figure 2, which displays a mediocre-resolution image of the "Cloverleaf", a gravitationally lensed quasar (Magain et al., 1988), together with the deconvolved version, using a sampling interval twice as short. The four lensed images, which were unresolved in the original data, are completely separated after deconvolution. The deduced fluxes are fully compatible with those measured on higher-resolution images and, although the original resolution is 1.3 arcsec only and the pixel size is 0.35 arcsec, the deduced image positions are accurate to 0.01 arcsec.

Figure 3 illustrates the deconvolution of an image of the compact star cluster Sk 157 in the Small Magellanic Cloud (Heydari-Malayeri et al., 1989). The original image was obtained with the ESO/MPI 2.2-m telescope at La Silla, in average seeing conditions (1.1 arcsec FWHM). While the original maximum entropy deconvolution (Heydari-Malayeri et al., 1989) allowed to resolve the cluster into 12 components, our new algorithm detects more than 40 stars in the same area.

Another important application of our algorithm is the simultaneous deconvolution of different images of the same field. These images may be obtained with the same instrument or with different ones. The solution is then a light distribution which is compatible with all the images considered. Our technique even allows to let, e.g., the intensities of the point sources converge to different values in the different images, so that variable objects may be considered. This should be very useful for the photometric monitoring of variable objects in crowded fields (e.g. Cepheids in distant galaxies).

Figure 4 illustrates this simultaneous deconvolution on simulated images, the first of which has a good resolution but a poor S/N (as might be obtained with a space telescope) and the second one a low-resolution and a high S/N (a typical image from a large ground-based telescope). Contrary to Lucy's method (Lucy, 1991) which is very sensitive to the noise present in one of the images, our technique allows to reliably recover both the high resolution of the space image and the hidden information content of the ground-based one.

In the same spirit, our algorithm is well adapted to the processing of images obtained with adaptive optics techniques. In the latter, numerous short exposures of the same field are usually obtained, the shape of the mirror being continuously adapted to correct for atmospheric distortions. So, the observations consist in a number of images of the same field, each of them having its own PSF. Performing a simple sum results in an image whose spatial resolution is typical of the average observing conditions, while a simultaneous deconvolution not only allows to take count of the best conditions, but even results in an improved resolution by optimally combining the information content of the different images. A simple illustration of these considerations is provided by Figure 5, which shows the simultaneous deconvolution of four adaptive-optics-like images of the same field, where the PSF as well as the image centring vary from one observation to the other.

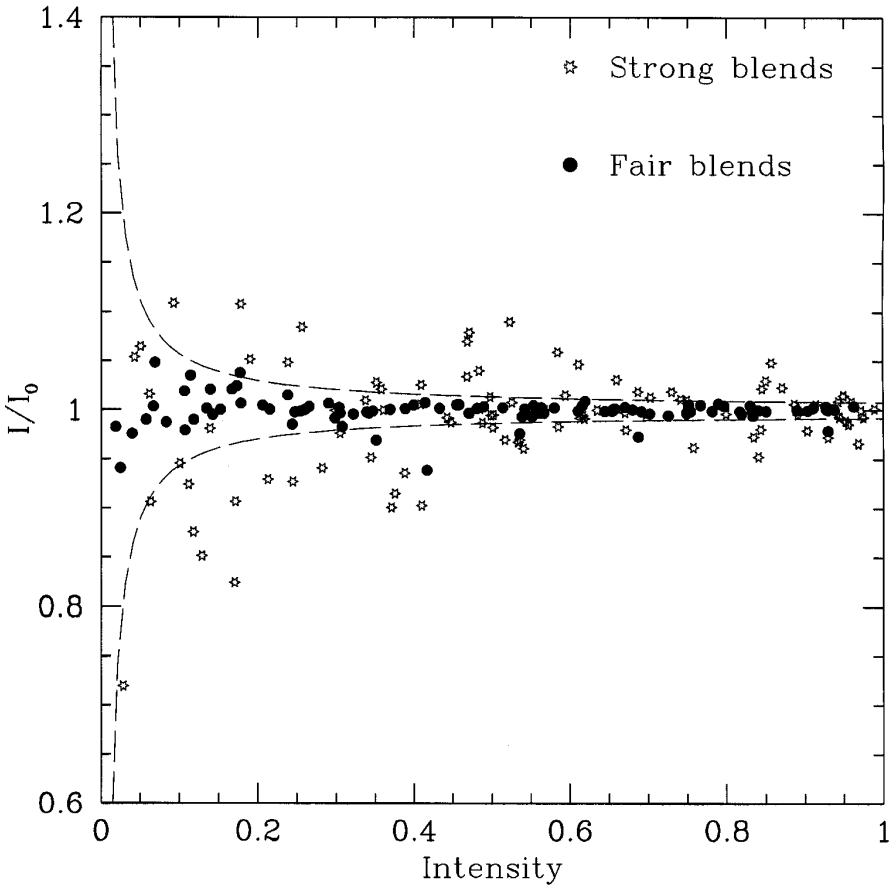

Figure 6: Photometric test performed on a synthetic field containing 200 stars with random positions and intensities, nearly all blended to various degrees. The relative errors are plotted against the total intensity (the latter being on an arbitrary scale, corresponding to an integrated S/N varying from 10 to 400). Open symbols represent heavily blended stars (the distance to the nearest neighbour is smaller than the FWHM), filled symbols correspond to less blended objects. The dashed curves are the theoretical 3σ errors for isolated stars, taking into account the photon noise alone.

Traditional deconvolution methods are notoriously unable to give photometrically accurate results. The main reasons are that (1) the rings which tend to be produced around point sources may interfere with neighbouring objects so that the flux is redistributed between the sources and (2) the smoothing recipe generally forces the stars to deviate as little as possible from the background, so that the intensity peaks are generally underestimated.

Our algorithm naturally avoids these two biases, as is illustrated in Figure 6, which shows the results of a photometric test applied to a synthetic field containing 200 stars in a 128×128 pixels image, nearly all the stars being blended to various degrees (197 stars out of 200 have the nearest neighbour within 2 FWHMs). Moreover, these stars are superimposed on a variable background. Figure 6 clearly shows that no systematic error is present, and that the intensities of all but the most severely blended objects are reproduced with errors compatible with the photon noise.

More details about the deconvolution technique and astronomical applications can be found at: http://vela.astro.ulg.ac.be/imaproc

References

Heydari-Malayeri, M., Magain, P., Remy, M. *Astron. Astrophys.* **222**, 41 (1989).

Lucy, L. *Astron. J.* **79**, 745 (1974).

Lucy, L. *ST-ECF Newsletter* **16**, 6 (1991).

Magain, P., Surdej, J., Swings, J.-P. et al. *Nature* **334**, 325 (1988).

Press, W.H., Flannery, B.P., Teukolsky, S.A. & Vetterling, W.T. *Numerical Recipes* (Cambridge University Press, 1989).

Richardson, W.H. *J. Opt. Soc. America* **62**, 55 (1972).

Shannon, C.J. *Proc. I.R.E.* **37**, 10 (1949).

P. Magain, F. Courbin
magain@astro.ulg.ac.be
courbin@astro.ulg.ac.be